Published in final edited form as:
Neurobiol Dis. 2013 August ; 56: 6–13. doi:10.1016/j.nbd.2013.04.003.

RNAi or overexpression: Alternative therapies for Spinocerebellar Ataxia Type 1

Megan S. Keiser[d], **James C. Geoghegan**[a], **Ryan L. Boudreau**[a], **Kim A. Lennox**[e], and **Beverly L. Davidson**[a,b,c,d,*]

[a]Department of Internal Medicine, University of Iowa, Iowa City, IA 52242, USA

[b]Department of Neurology, University of Iowa, Iowa City, IA 52242, USA

[c]Department of Physiology and Biophysics, University of Iowa, Iowa City, IA 52242, USA

[d]Department of the Neuroscience Training Program, University of Iowa, Iowa City, IA 52242, USA

[e]Integrated DNA Technologies Inc., Coralville, IA 52241, USA

Abstract

Spinocerebellar Ataxia Type 1 (SCA1) is an autosomal dominant late onset neurodegenerative disease caused by an expanded polyglutamine tract in ataxin-1. Here, we compared the protective effects of overexpressing ataxin-1-like using recombinant AAVs, or reducing expression of mutant ataxin-1 using virally delivered RNA interference (RNAi), in a transgenic mouse model of SCA1. For the latter, we used an artificial microRNA (miR) design that optimizes potency, efficacy and safety to suppress ataxin-1 expression (miS1). Delivery of either ataxin-1-like or miS1 viral vectors to SCA1 mice cerebella resulted in widespread cerebellar Purkinje cell transduction and improved behavioral and histological phenotypes. Our data indicate the utility of either approach as a possible therapy for SCA1 patients.

Keywords

Spinocerebellar Ataxia Type 1; Ataxin-1; Ataxin-1-like; miRNA; RNAi; AAV; Cerebellum; Neurodegeneration; Polyglutamine

Introduction

Spinocerebellar Ataxia Type 1 (SCA1) is a late onset, autosomal dominant neurodegenerative disease caused by a polyglutamine (polyQ) expansion in the ataxin-1 protein. The average age of onset is within the fourth decade of life, although juvenile cases have been documented (Zoghbi et al., 1988). Cell death in the cerebellar Purkinje cells and brain stem neurons is characteristic of SCA1 (Orr et al., 1993; Zoghbi and Orr, 1995). Although not fully understood, mechanisms underlying neuropathy include an interplay

*Corresponding author at: University of Iowa, Department of Internal Medicine, Room 200, Eckstein Medical Research Building, Iowa City, IA 52242, USA. Fax:+1 319 353 5572. beverly-davidson@uiowa.edu (B.L. Davidson).

Supplementary data to this article can be found online at http://dx.doi.org/10.1016/j.nbd.2013.04.003.

between ataxin-1 and several proteins including 14-3-3 (Chen et al., 2003), Rbm17 (Lim et al., 2008), Capicua (Lam et al., 2006) and Ataxin-1-like (Mizutani et al., 2005).

The B05 transgenic mouse model of SCA1 expresses a polyQ expanded human ataxin-1 allele under control of the Purkinje cell specific promoter (Pcp2) (Burright et al., 1995). Purkinje cell death occurs at approximately 24 weeks of age, with behavioral deficit onset at 5 weeks (Clark et al., 1997). This implies that early symptoms reflect neuronal dysfunction but not overt cell loss, and raises the possibility that therapy can be initiated after disease onset. Work by Orr and colleagues using a doxycycline-inducible system investigated this possibility and found that if the disease gene was turned off after 6 weeks of expression, there was full reversibility. Notably, partial restoration of neuronal and behavioral deficits occurred if gene expression was turned off after 12 weeks (Zu et al., 2004). Thus, there is a window of opportunity after disease onset to which therapies may have benefit.

Therapeutic intervention for SCA1 may involve small molecule approaches, such as those which have been investigated for SCA2 (Velazquez-Perez et al., 2011), modulation of disease through overexpression of ataxin-1-like (Bowman et al., 2007), or reducing expression of the disease allele through gene silencing (Alves et al., 2008; Gonzalez-Alegre et al., 2005). In SCA1 knock-in mice (154Q) overexpressing an ataxin-1-like-transgenic allele, disease phenotypes improved (Lim et al., 2008). The presumed mechanism for therapy based on ataxin-1-like overexpression is that ataxin-1-like, ataxin-1 andmutant, polyQ-expanded ataxin-1 all interactwith Capicua through their AXH domain (de Chiara et al., 2003; Lam et al., 2006; Lim et al., 2008). Interestingly, ataxin-1-like does not have a polyQ region but if overexpressed *in vitro* it can effectively compete away the mutant ataxin-1:Capicua interactions (Bowman et al., 2007). A separate study showed that Rbm17 competes with Capicua to bind ataxin-1, with Rbm17 favoring interactions with mutant, polyQ-expanded ataxin-1, thus contributing to the toxic gain-of-function phenotype (Bowman et al., 2007). To date, interactions between Rbm17 and ataxin-1-like have not been reported.

Modulating SCA1 pathogenesis through gene silencing takes advantage of the RNA interference (RNAi) pathway, a naturally occurring process that regulates expression through genomically encoded small RNAs, which include microRNAs (miRs). RNAi has been utilized as a means to reduce target gene expression for potential treatment of various diseases (Davidson and McCray, 2011), including the dominantly inherited gain of function mutations underlying SCA1 and Huntington's disease (Boudreau et al., 2009b; Harper et al., 2005; Xia et al., 2004). In earlier work, we established that siRNAs processed from short hairpin RNAs (shRNAs) expressed from viral vectors could reduce targets in brain (Xia et al., 2002, 2004) and could improve disease phenotypes in SCA1 transgenic mice (Xia et al., 2004).

Here, we take advantage of recent improvements in expression systems and siRNA design to deliver RNAi triggers that are appropriately expressed *in vivo* and possess low off targeting potential (Boudreau et al., 2009, 2011; McBride et al., 2008). We test their therapeutic utility in the B05 mouse model, and compare this approach with ataxin-1-like overexpression *via* viral vectors.

Materials and methods

Plasmids and viral vectors

The plasmid expressing mouse U6-driven artificial miRNA, miS1, was cloned as previously described using DNA oligonucleotides (Boudreau et al., 2008). Artificial miRNA expression cassettes were cloned into pAAVmcsCMVeGFP plasmids which coexpressed CMV-driven eGFP (Boudreau et al., 2009a).

Human ataxin-1-like was originally cloned from HEK293 cells using forward primer 5′ AAACCTGTTCATGAAA and reverse primer 5′ GGATCCTCATTTTCCCGCATTGGAAC containing a BamHI site and cloned into pCR4-TOPO plasmid (Life Technologies, Grand Island, NY). The sequence was expanded to contain a NheI site, a Flag tag and kozak sequence by consecutive PCR extensions using forward primers: *a*) 5′ ATAAAGATCATGATATCGATTACAAGGATGACGATGACA AACCTGTTCAT; and *b*) GCTAGCGCCACCATGGACTACAAAGACCATGA CGGTGATTATAAGATCAT. Sequential digests were conducted with BamHI and NheI followed by CIP treatment and electrophoresis of the digested product. The DNA construct band was purified using a QIAquick Gel Extraction Kit (Qiagen, Valencia, CA) per manufacturer's protocol. The purified DNA insert was ligated (T4 DNA Ligase; NEB, Ipswich, MA) into pFBAAVmcsBGHpA pre-digested with BamHI and NheI (McLoughlin et al., 2012). EF1α was cloned from pBUD plasmid using forward primer 5′ TTAATTAAGTGAGGCTCCGGTGCCCGTC containing a PacI site and reverse primer 5′ GCTAGCGCCAGATC TCTCGAGTCCAC containing a NheI site into pCR™4-TOPO® plasmid (Life Technologies, Grand Island, NY). EF1α was digested with PacI and NheI, gel purified and ligated into pFBAAVmcsBGHpA upstream of flag-tagged human ataxin-1-like.

Recombinant AAV serotype 2/1 vectors (AAV.miC.eGFP, AAV.miS1.eGFP, and AAV.HAtxn1L) were generated by the University of Iowa Vector Core facility as previously described (Urabe et al., 2002). AAV vectors were resuspended in Formulation Buffer 18 (University of Iowa Gene Transfer Vector Core, Iowa City, IA) and titers (viral genomes/ml) were determined by quantitative PCR (qPCR).

Cell culture and transfection

HEK293 cells were transfected (Lipofectamine™ 2000, Life Technologies, Grand Island, NY) in triplicate in 24-well plates per manufacturer's instructions with 800 ng of pFBAAVmcsBGHpA plasmid containing the human ataxin-1-like construct, pAAVCMVeGFP, pAAV, or no plasmid. Total RNA was harvested 48 h later with TRIzol® (Life Technologies, Grand Island, NY).

Animals

All animal protocols were approved by the University of Iowa Animal Care and Use Committee. Wild type FVB mice were obtained from Jackson Laboratories (Bar Harbor, ME). SCA1-1 TM (line B05) mice were generously provided by Dr. H.T. Orr (Burright et al., 1995) and the B05 line was maintained on the FVB background. Mice were genotyped using primers specific for the mutant human ataxin-1 transgene (Burright et al., 1995), and

hemizygous and age-matched wild type littermates were used for the indicated experiments. In the therapeutic trials, the treatment groups comprised approximately equal numbers of male and female mice. Mice were housed in a controlled temperature environment on a 12-hour light/dark cycle. Food and water were provided *ad libitum*.

AAV injections and brain tissue isolation

B05 mice were injected with AAV vectors as previously reported (McBride et al., 2008). For all studies mice were injected bilaterally into the deep cerebellar nuclei (coordinates −6.0 mm caudal to bregma, ±2.0 mm from midline, and −2.2 mm deep from cerebellar surface) with 4 μl of AAV1 virus (at 1×10^{12} viral genomes/ml) or saline (Formulation Buffer 18). Mice were anesthetized with a ketamine/xylazine mix and transcardially perfused with 20 ml of 0.9% cold saline. Mice were decapitated, and for histological analyses, brains were removed and post-fixed overnight in 4% paraformaldehyde. Brains were stored in a 30% sucrose/0.05% azide solution at 4 °C until cut on a sliding knife microtome at 60 μm thickness and stored at −20 °C in a cryoprotectant solution. For ISH, brains were put in OCT (Sakura Finetek USA) and frozen in slurry of dry ice and 70% ethanol, then kept at −80 °C until cut on a cryostat at 10 μm thickness and stored at −80 °C. For qPCR analyses, brains were removed, sectioned into 1 mm thick coronal slices using a brain matrix (Roboz, Gaithersburg, MD) and eGFP expression was verified. Whole cerebellum was triturated in 100 μl of TRIzol® (Life Technologies, Grand Island, NY) and flash frozen in liquid nitrogen and stored at −80 °C until used. RNA was isolated from whole cerebellum using 1 ml of TRIzol®. RNA quantity and quality were measured using a NanoDrop® ND-1000 (NanoDrop, Wilmington, DE).

Immunohistochemical analyses

Free-floating sagittal cerebellar sections (60 μm thick) were washed in 1 × PBS at room temperature and blocked for 1 h in 10% serum, 0.03% Triton-100 in 1 × PBS. Sections were incubated with primary antibody in 2% serum and 0.03% Triton-X in 1 × PBS overnight at 4 °C. Primary antibodies used were polyclonal anti-Iba1 (1:1000; WAKO, Richmond, VA) and polyclonal rabbit anti-Calbindin (1:2000; Cell Signaling Technology, Danvers, MA). For fluorescent IHC, sections were incubated with goat anti-rabbit Alexa Fluor 568 (1:1000; Life Technologies, Grand Island, NY) in 2% serum and 0.03% Triton-100 in 1 × PBS for 1 h at room temperature. For DAB IHC, sections were incubated in goat anti-rabbit biotin-labeled secondary antibody (1:200; Jackson Immunoresearch) in 2% serum and 0.03% Triton-X at room temperature for 1 h. Tissues were developed with VECTASTAIN® ABC Elite Kit (Vector Laboratories, Burlingame, CA), according to the manufacturer's instructions. All sections were mounted onto Superfrost Plus slides (Fischer Scientific, Pittsburgh, PA) and cover slipped with Fluoro-Gel (Electron Microscopy Sciences, Hatfield, PA). Images were captured on Leica Leitz DMR fluorescence microscope connected to an Olympus DP72 camera using the Olympus DP2-BSWsoftware (Olympus, Melville, NY).

In situ hybridization

A 2′OMe ZEN probe (Integrated DNA Technologies, Coralville, IA) was used to visually localize miS1 by *in situ* hybridization (ISH) designed to the reverse complement of the

targeted miS1 mRNA (5′ Dig-AzAGCAACGACCUGAAGAUCGzA-Dig 3′. Where AGCU = 2′OMe RNA, Dig = Digoxigenin, and z = ZEN modifier). AAV.miS1.eGFP injected samples were verified for expression by eGFP fluorescence before treatment. Sections were treated by ISH methods previously described (McLoughlin et al., 2012).

Semi-quantitative PCR

Reverse transcription (High Capacity cDNA Reverse Transcription Kit, Applied Biosystems, Foster City, CA) was performed on total RNA collected from cerebellum using a standard stem-loop PCR primer (Chen et al., 2005) designed to identify miS1 (5′ GTCGTATCCAGTGCAG GGTCCGAGGTATTCGCACTGGATACGACAGCAAC). cDNA was subjected to RT-PCR with a standard reverse primer (5′ GTGCAGGGTCCGAGGT) and a forward primer (5′ ACACTCCAGCTGGGTCGATCTTCAGGTC) to identify miS1 expression.

Western blot analysis

Protein was harvested from transfected HEK293 cells or whole cerebellar lysates using RIPA buffer (ThermoScientific Pierce, Rockford, IL) and 1 × protease inhibitor using standard techniques and quantified using D_C™Protein Assay (Bio-Rad, Hercules, CA). Protein extracts were separated on a 7% acrylamide gel and transferred to Immobilon-P PDVF transfer membranes (MerckMillipore, Billerica,MA). Primary antibody to Flag (1:500; Sigma-Aldrich, St. Louis, MO) and β-Actin (1:10,000; Sigma-Aldrich, St. Louis, MO) were used. Blots were developed using ECL Plus Western Blotting Detection System (GE Healthcare Life Sciences, Pittsburgh, PA).

Co-immunoprecipitation analysis

Saline perfused cerebellum from either injected or control non-injected B05 mice were dounce homogenized in ice-cold TST buffer (50 mM Tris pH 8.0, 75 mM NaCl, 0.5% Triton-X 100, 1 mM PMSF) containing complete mini protease inhibitors (Roche Applied Science, Indianapolis, IN). Lysates were solubilized on ice for 1 h and then clarified by centrifugation at 16 K ×*g* for 10 min at 4 °C. For anti-flag/ataxin-1-like immunoprecipitations, 2 mg of protein from the supernatant samples was combined with 20 μl of packed anti-flag M2 magnetic beads (Sigma-Aldrich) and allowed to incubate overnight on a rotator at 4 °C. Using a magnet, the beads were washed three times with ice-cold Wash Buffer (50 mM Tris pH 7.4, 150 mM NaCl). Bound proteins were eluted by heating in 2× LDS sample buffer (Life Technologies, Grand Island, NY) for 10 min at 70 °C. Input and elution samples were analyzed by SDS-PAGE and western blotting. Flag tagged ataxin-1-like was detected with rabbit anti-flag primary antibody (1:1000; Cell Signaling Technology, Danvers, MA) and ataxin-1 was detected with rabbit anti-ataxin-1 11750 V primary antibody. HRP-conjugated goat anti-rabbit secondary antibody (1:2000; Cell Signaling Technology, Danvers, MA) was used for ECL detection.

Quantitative PCR

Random-primer first-strand cDNA synthesis was performed using 1 μg total RNA (High Capacity cDNA Reverse Transcription Kit; Life Technologies, Grand Island, NY) per

manufacturer's instructions. Assays were performed on a sequence detection system using primers/probe sets specific for human ataxin-1, mouse GFAP, mouse Calbindin, or mouse β-Actin (ABI Prism® 7900 HT and TaqMan® 2× Universal Master Mix; Life Technologies, Grand Island, NY).

Behavioral analysis

All assays were performed at 37 weeks of age and presented as means ± SEM unless otherwise specified. Uninjected wild type, $n = 14$; saline injected B05, $n = 8$; AAV.miC.eGFP injected B05, $n = 11$; AAV.miS1.eGFP injected B05, $n = 13$; and AAV.HAtxn1L injected B05, $n = 10$ mice per group.

Ledge test and hindlimb clasping

Assays and their scoring parameters are detailed previously (Guyenet et al., 2010).

Stride length measurements

Mice were allowed to walk across a paper-lined chamber (100 cm × 10 cm with 10 cm walls) and into an enclosed recess. Mice were given one practice run. Non-toxic red and blue paint was applied to their fore- and hindpaws, respectively. Mice were then tested three times to produce three separate footprint tracings. Stride lengths were measured from the middle of each paw print between the same paws for steps taken during their gait. Steps were discarded in instances where a mouse stopped walking or turned around. Measurements were averaged for all four paws and data were presented as box plots.

Rotarod performance

Mice were tested on an accelerated rotarod apparatus (model 47600; Ugo Basile, Comerio, Italy) at 4, 27 and 37 weeks of age. Baseline testing was conducted at 4 weeks of age to separate B05 mice equally into treatment groups. No difference between B05 and wild type mice was seen at 4 weeks of age (data not shown). Mice were first habituated on the rotarod for 4 min. Mice were then tested three trials per day (with at least 30 min of rest between trials) for four consecutive days. For each trial, acceleration was from 4 to 40 rpm over 5 min, and then speed maintained at 40 rpm. Latency to fall (or if mice hung on for two consecutive rotations without running) was recorded for each mouse per trial. The trials were stopped at 500 s, and mice remaining on the rotarod at that time were scored as 500 s. Two-way analysis of variance followed by Bonferroni *post-hoc* analysis was used to assess for significant differences. Variables were time and treatment.

Statistical analyses

For all studies, p values were obtained by using one-way analysis of variance followed by Bonferroni *post-hoc* analysis to assess for significant differences between individual groups unless indicated otherwise. Student's t-test was used for the pair-wise comparisons for the baseline 4-week rotarod performance assay in untreated mice. In all statistical analyses, $P < 0.05$ was considered significant.

Figure preparation

All photographs were formatted with Adobe Photoshop software, all graphs were made with Prism Graph software, and all figures were constructed with Adobe Illustrator software.

Results

Experimental design: optimization and validation of therapeutic delivery

Two vectors were generated to test alternative therapies; AAV expressing a siRNA against human ataxin-1 or AAVs expressing human ataxin-1-like. While earlier work in our group demonstrated short term efficacy using an RNAi approach in the B05 model (Xia et al., 2004), we have substantially improved the safety of vector-based platforms by moving from shRNA systems to those based on endogenous miRNA backbones (Boudreau and Davidson, 2012; Boudreau et al., 2008, 2009a, 2012; McBride et al., 2008). For this work, we also took advantage of recent progress in minimizing off-sequence silencing to design an RNAi trigger that would target human ataxin-1 but have low off-target potential (Boudreau et al., 2009a, 2011). Our sequence targeting human ataxin-1 (miS1) was cloned into shuttle plasmids also expressing eGFP, and then subsequently packaged into AAV2/1 (AAV.miS1.eGFP). Human ataxin-1-like cDNA was modified to contain an N-terminal 3× Flag tag and subsequently cloned downstream of the EF1α promoter for packaging in AAV2/1 (AAV.HAtxn1L) (Fig. 1A).

AAV.miS1.eGFP, AAV.HAtxn1L, AAV.miC.eGFP (control miRNA sequence within AAV2/1) or saline was injected bilaterally into the deep cerebellar nuclei (DCN) of 5 week old B05 mice to confirm either gene silencing activity or human ataxin-1-like overexpression, respectively. Tissue was harvested for RNA or protein extraction 3 weeks later. Q-RT-PCR showed 30% knockdown of human ataxin-1 mRNA levels compared to control injected B05 mice ($p < 0.0001$; Supplementary Fig. 1A). Ataxin-1-like expression was verified by western blot analysis of either transfected HEK293 cells or B05mice injected previously with AAV.HAtxn1L into the DCN (Supplementary Fig. 1B).

At 40 weeks of age, harvested tissues showed robust eGFP expression throughout rostral and caudal lobules of AAV.miS1.eGFP injected cerebella (Fig. 1B). Stem-loop PCR has been used previously to examine expression of endogenously expressed miRNAs (Chen et al., 2005; Tang et al., 2006). We designed specific probes to similarly test for expression of miS1 in total RNA harvested from cerebellar extracts. Stem-loop PCR confirmed that miS1 was expressed in AAV.miS1.eGFP injected animals (Fig. 1C), but not those injected with AAV.miC.eGFP. *In situ* hybridization using probes specific for the guide strand of the miRNA liberated from the artificial miR platform demonstrated miS1 expression predominantly in Purkinje cells of AAV.miS1.eGFP treated mice (Fig. 1D). Q-RT-PCR on RNA harvested from whole cerebellar extracts showed a 70% reduction of human ataxin-1 mRNA levels in AAV.miS1.eGFP treated animals relative to controls and AAV.HAtxn1L injected mice (Fig. 1E).

By immunohistochemical analysis, calbindin, a Purkinje cell marker, is reduced in 6 week old B05 mice compared to wild type littermates (Vig et al., 1998, 2000), and was therefore used as a surrogate marker for recovery of Purkinje cell viability. Here, we assessed

calbindin transcript levels using Q-RT-PCR. Although there were not significant differences between control treated B05 mice and wild type littermates, AAV.miS1.eGFP animals had significantly higher calbindin mRNA levels relative to all other B05 treatment groups ($p < 0.001$; Fig. 1F).

Ataxin-1-like over-expression and knockdown of ataxin1 rescues behavioral phenotypes

The B05 mouse model displays many characteristics of human SCA1 patients including impaired gait, balance, and overall motor coordination as well as hindlimb muscle atrophy (Burright et al., 1995). The ledge test measures coordination, which is compromised in the cerebellar ataxias (Guyenet et al., 2010). As expected, control treated animals performed significantly worse than all other groups ($p < 0.0001$). Remarkably, there were no significant differences between AAV.miS1.eGFP or AAV.HAtxn1L-treated animals and their wild type littermates. Both ataxin-1 suppression and overexpression of human ataxin-1-like rescued the balance, agility, and hindlimb musculature needed to perform this task to the same level of coordination as wild type littermates (Fig. 2A).

SCA1 mice display hindlimb clasping whereas wild type mice generally splay their hindlimbs (Chou et al., 2008). At 37 weeks of age AAV.miS1.eGFP and AAV.HAtxn1L-treated animals treated mice showed significant improvements with reduced clasping of one or both hindlimbs relative to control-treated B05 mice ($p < 0.0001$). Again, there was no significant difference between AAV.miS1.eGFP or AAV.HAtxn1L- treated animals and their wild type littermates, who spent the vast majority of time with their hindlimbs splayed (Fig. 2B).

Gait analysis has been used as a phenotypic measure of disease in SCA1 mice (Clark et al., 1997), and as a marker of rescue in HD mice subjected to RNAi therapy (Harper et al., 2005). While wild type mice had significantly longer stride lengths than all other groups at 37 weeks of age (Fig. 2C; $p < 0.0001$). AAV.miS1.eGFP and AAV.HAtxn1L treated animals had significantly longer strides (6–8 mm) than control treated B05 mice ($p < 0.0001$; Fig. 2C), suggesting partial rescue of the gait phenotype with either therapy. There was no significant difference between AAV.miS1.eGFP or AAV.HAtxn1L treated animals.

Mice were also tested on the accelerating rotarod at 27 and 37 weeks of age. At 27 weeks of age, AAV.miS1.eGFP or AAV.HAtxn1L treated animals stayed on the accelerated rotarod 100–150 s longer than AAV.miC.eGFP or saline treated B05 animals ($p < 0.05$;Fig. 2D). At 37 weeks of age AAV.miC.eGFP and saline injected groups of B05 mice were indistinguishable from each other and were significantly worse than AAV.miS1.eGFP or AAV.HAtxn1L treated B05 mice or their wild type littermates by two-way ANOVA ($p < 0.05$; Fig. 2D). Notably, mice in the AAV.miS1.eGFP or AAV.HAtxn1L treatment groups, and wild type mice, remained on the accelerated rotarod approximately 2 min longer than control treated B05 mice. Also, there was no significant difference between therapeutically treated B05 mice and wild type animals in their latency to fall. These results indicate that, even at extended time points, mice treated with miS1 or human ataxin-1-like perform with the same level of motor coordination as wild type animals, and demonstrated rescue of the rotarod phenotype (Fig. 2D).

Analysis of in vivo protein interactions with overexpressed ataxin-1-like

Polyglutamine expansion in ataxin-1 yields a toxic gain-of-function *via* enhanced complex formation with Rbm17 (Lim et al., 2008). Given this, we were interested to know whether overexpressed ataxin-1-like can also interact with Rbm17 *in vivo*. Consistent with previous studies, we found that ataxin-1 and exogenously expressed ataxin-1-like co-immunoprecipitate using cerebellar extracts from B05 mice injected with AAV.HAtxn1L (Supplementary Fig. 2). However, unlike ataxin-1, Rbm17 did not co-immunoprecipitate with ataxin-1-like in either Rbm17 or ataxin-1-like immunoprecipitates (data not shown).

Treatment with AAV.HAtxn1L or AAV.miS1 is not toxic in vivo

Iba1 is an antigen often used to assess microglia activation, as can occur in the setting of toxic shRNAs (McBride et al., 2008). Iba1 staining was not different among the groups, and there was no evident neurotoxicity in AAV.miS1.eGFP or AAV.HAtxn1L injected animals compared to wild type littermates, either at the injection site (DCN) or remotely in cerebellar lobules (Fig. 3A). Levels of GFAP, an astrocytic marker, were measured by Q-RT-PCR on RNA isolated from whole cerebellar extracts (Fig. 3B). AAV.miS1.eGFP and AAV.HAtxn1L treated animals had no significant increases in GFAP mRNA levels compared to saline treated animals. AAV.miC.eGFP injected animals had elevated GFAP levels relative to all other treatment groups ($p < 0.05$).

Ataxin-1-like overexpression and human ataxin-1 knockdown improves neuropathology

Dendritic pruning in Purkinje cells is an early phenotype in B05 mice (Burright et al., 1995). Molecular layer width provides quantitative insight into dendritic integrity and overall Purkinje cell viability. Sagittal cerebellar sections were stained for the Purkinje cell marker Calbindin, and molecular layer width quantified in transduced cerebellar lobules IV/V and VI. B05 mice treated with AAV.miS1.eGFP or AAV.HAtxn1L showed partial rescue of the thinned molecular layer width compared to control treated B05 mice ($p < 0.0001$; (Figs. 4A, B).

Ectopic Purkinje cells are present by 16 weeks of age in B05 mice, with Purkinje cell death evident by 24 weeks (Burright et al., 1995). We found partial but significant rescue in the numbers of Purkinje cells retained after AAV.miS1.eGFP or AAV.HAtxn1L treatment ($p < 0.0001$; Fig. 4C), and a marked reduction in ectopic Purkinje cell numbers ($p < 0.0001$; Fig. 4D). Indeed, for ectopic Purkinje cell counts among the B05 groups, there was no difference between AAV.miS1.eGFP or AAV.HAtxn1L treated mice and their wild type littermates. Thus, the partial histological rescue of molecular layer width and Purkinje cell number, but improved ectopic Purkinje cell phenotypes, suggests that behavioral recovery does not require full rescue of all neuropathological aspects.

Discussion

Here we demonstrate two different therapeutic approaches that improve disease phenotypes in B05 transgenic SCA1 mice. Silencing of mutant ataxin-1 using miRNAs or, alternatively, overexpression of ataxin-1-like both rescued behavioral deficits and improved the well-documented neuropathology in B05 mice. Previous work from our lab using early

generation shRNAs showed that RNAi provided therapeutic benefit in this model in short term experiments. Here, using improved methodology we designed a safer and more potent miRNA, miS1, which achieved 70% knockdown of human ataxin-1 *in vivo* for extended time points (35 weeks post-injection), improved B05 neuropathy and rescued motor deficits while showing no adverse effects.

Previous work using a transgenic approach demonstrated that doubling endogenous levels of mouse ataxin-1-like improved phenotypes and neuropathy in the SCA1 knock-in model (Bowman et al., 2007). Here we showed that viral-mediated overexpression of ataxin-1-like delivered after cerebellar development improved motor and neuronal phenotypes in the B05 model. Overexpression of human ataxin-1-like was comparable to SCA1 phenotypic rescue by suppression of the mutant human ataxin-1 transgene.

It is well established that degeneration of Purkinje cell dendrites occurs long before Purkinje cell death in SCA1 pathogenesis (Burright et al., 1995; Clark et al., 1997; Klement et al., 1998). At later stages (24 weeks) in disease progression in B05 mice there is a significant reduction in the number of Purkinje cells and noticeable ectopic localization of remaining Purkinje cells (Clark et al., 1997). B05 mouse cerebella develop normally, thus ectopic cells are not due to a developmental migratory deficit. Rather the Purkinje cells likely translocate from their normal position to maintain distal dendritic association with parallel fibers in the superficial molecular layer (Clark et al., 1997). Both AAV.miS1.eGFP and AAV.HAtxn1L treatment rescued the ectopic Purkinje cell phenotype. This, in addition to the partial rescue of dendritic integrity indicated by the retention of molecular layer width suggests that both therapeutic approaches improve multiple aspects of known cerebellar neuropathy in SCA1.

Partial rescue of rotarod phenotypes, early in disease, occurred *via* duplication of ataxin-1-like in the knock-in model (Bowman et al., 2007), and partial rescue using shRNAs was seen at 21 weeks in B05 mice (Xia et al., 2004). Here, we found full rotarod rescue at late time points, an important consideration for moving this platform into clinical application. We also made the original observation that SCA1 mice have a phenotype in the ledge test, a useful assay to further query balance, agility, coordination and hindlimb musculature. Moreover, we demonstrate full rescue in the ledge test phenotype with either treatment modality. Together with our histological studies, we find that rescue of motor deficits occurs in the absence of complete normalization of histological readouts.

Capicua, a transcriptional repressor, interacts with ataxin-1. Capicua binds ataxin-1 when serine 776 (S776) is not phosphorylated regardless of polyQ tract length. Complete loss of ataxin-1 decreases Capicua protein levels, and normal Capicua repressor activity is modulated when bound to mutant ataxin-1 (Lam et al., 2006). Recently it was demonstrated that polyQ-expanded ataxin-1 alters Capicua's activity at specific transcriptional targets (Fryer et al., 2011). SCA1 knock-in mouse data suggest that polyQ-expanded ataxin-1:Capicua interactions induce hyper-repression. Concomitantly, this reduces Capicua binding to other targets (Fryer et al., 2011).

Important to this study, Capicua contains an AXH domain (Lam et al., 2006) and can bind ataxin-1 and ataxin-1-like. Early work tested the hypothesis that ataxin-1-like

overexpression competes with polyQ expanded ataxin-1, displaces the mutant protein, and allows its aggregation into a less toxic form (Bowman et al., 2007). Ataxin-1-like could mimic normal ataxin-1, bind Capicua and ablate the transcriptional modulation caused by polyQ-expanded ataxin-1: Capicua interaction. Whether phenotypic rescue in this study was the direct result of displaced mutant ataxin-1 or restoration of normal Capicua function is an interesting question and requires the development of tools to address their *in vivo* interactions.

Earlier work showed that Rbm17 complexes with phosphorylated S776 ataxin-1 with a preference to bind polyQ-expanded ataxin-1 over wild type ataxin-1 (Lim et al., 2008). In our study, exogenously expressed ataxin-1-like co-immunoprecipitated with ataxin-1, but not Rbm17. The lack of observed interaction between ataxin-1-like and Rbm17 suggests that these two proteins either do not interact *in vivo* or that the interaction is too weak or transient to be detected in our co-IP assay. The lack of an *in vivo* interaction between Rbm17 and ataxin-1-like is consistent with a model proposed by the Zoghbi lab (Lam et al., 2006), wherein ataxin-1-like overexpression restores normal Capicua activity. However, it is also possible that overexpressed ataxin-1-like sequesters mutant ataxin-1, thereby abrogating the toxic gain-of-function caused by the ataxin-1/Rbm17 complex formation. Although the mechanism of rescue from overexpression of human ataxin-1-like is not fully understood, the results of our study indicate the ataxin-1-like is a promising candidate for further pre-clinical experiments in SCA1 therapies.

Supplementary Material

Refer to Web version on PubMed Central for supplementary material.

Acknowledgments

The authors thank Dr. H Orr for his gift of ataxin-1 antibody 11750 V for IP analysis. This work was funded by the Roy J. Carver Trust (to B.L.D.) and the NIH (HD 44093, DK54759). The authors would also like to thank Stephanie Coffin for her assistance.

References

Alves S, et al. Allele-specific RNA silencing of mutant ataxin-3 mediates neuroprotection in a rat model of Machado-Joseph disease. PLoS One. 2008; 310:e3341. [PubMed: 18841197]

Boudreau RL, Davidson BL. Generation of hairpin-based RNAi vectors for biological and therapeutic application. Methods Enzymol. 2012:507275–507296.

Boudreau RL, et al. Minimizing variables among hairpin-based RNAi vectors reveals the potency of shRNAs. RNA. 2008; 149:1834–1844. [PubMed: 18697922]

Boudreau RL, et al. Artificial microRNAs as siRNA shuttles: improved safety as compared to shRNAs *in vitro* and *in vivo*. Mol. Ther. 2009a; 171:169–175. [PubMed: 19002161]

Boudreau RL, et al. Nonallele-specific silencing of mutant and wild-type huntingtin demonstrates therapeutic efficacy in Huntington's disease mice. Mol. Ther. 2009b; 176:1053–1063. [PubMed: 19240687]

Boudreau RL, et al. Rational design of therapeutic siRNAs: minimizing off-targeting potential to improve the safety of RNAi therapy for Huntington's disease. Mol. Ther. 2011; 1912:2169–2177. [PubMed: 21952166]

Boudreau RL, et al. siSPOTR: a tool for designing high specific and potent siRNAs for human and mouse. Nucleic Acids Res. 2012; 411:e9. [PubMed: 22941647]

Bowman AB, et al. Duplication of Atxn1l suppresses SCA1 neuropathology by decreasing incorporation of polyglutamine-expanded ataxin-1 into native complexes. Nat. Genet. 2007; 393:373–379. [PubMed: 17322884]

Burright EN, et al. SCA1 transgenic mice: a model for neurodegeneration caused by an expanded CAG trinucleotide repeat. Cell. 1995; 826:937–948. [PubMed: 7553854]

Chen HK, et al. Interaction of Akt-phosphorylated ataxin-1 with 14-3-3 mediates neurodegeneration in spinocerebellar ataxia type 1. Cell. 2003; 1134:457–468. [PubMed: 12757707]

Chen C, et al. Real-time quantification of microRNAs by stem-loop RT-PCR. Nucleic Acids Res. 2005; 3320:e179. [PubMed: 16314309]

Chou AH, et al. Polyglutamine-expanded ataxin-3 causes cerebellar dysfunction of SCA3 transgenic mice by inducing transcriptional dysregulation. Neurobiol. Dis. 2008; 311:89–101. [PubMed: 18502140]

Clark HB, et al. Purkinje cell expression of a mutant allele of SCA1 in transgenic mice leads to disparate effects on motor behaviors, followed by a progressive cerebellar dysfunction and histological alterations. J. Neurosci. 1997; 1719:7385–7395. [PubMed: 9295384]

Davidson BL, McCray PB Jr. Current prospects for RNA interference-based therapies. Nat. Rev. Genet. 2011; 125:329–340. [PubMed: 21499294]

de Chiara C, et al. The AXH module: an independently folded domain common to ataxin-1 and HBP1. FEBS Lett. 2003:5511–5513. 107–112.

Fryer JD, et al. Exercise and genetic rescue of SCA1 *via* the transcriptional repressor Capicua. Science. 2011; 3346056:690–693. [PubMed: 22053053]

Gonzalez-Alegre P, et al. Silencing primary dystonia: lentiviral-mediated RNA interference therapy for DYT1 dystonia. J. Neurosci. 2005; 2545:10502–10509. [PubMed: 16280588]

Guyenet SJ, et al. A simple composite phenotype scoring system for evaluating mouse models of cerebellar ataxia. J. Vis. Exp. 2010; 39

Harper SQ, et al. RNA interference improves motor and neuropathological abnormalities in a Huntington's disease mouse model. Proc. Natl. Acad. Sci. U. S. A. 2005; 10216:5820–5825. [PubMed: 15811941]

Klement IA, et al. Ataxin-1 nuclear localization and aggregation: role in polyglutamine-induced disease in SCA1 transgenic mice. Cell. 1998; 951:41–53. [PubMed: 9778246]

Lam YC, et al. ATAXIN-1 interacts with the repressor Capicua in its native complex to cause SCA1 neuropathology. Cell. 2006; 1277:1335–1347. [PubMed: 17190598]

Lim J, et al. Opposing effects of polyglutamine expansion on native protein complexes contribute to SCA1. Nature. 2008; 4527188:713–718. [PubMed: 18337722]

McBride JL, et al. Artificial miRNAs mitigate shRNA-mediated toxicity in the brain: implications for the therapeutic development of RNAi. Proc. Natl. Acad. Sci. U. S. A. 2008; 10515:5868–5873. [PubMed: 18398004]

McLoughlin HS, et al. Dicer is required for proliferation, viability, migration and differentiation in corticoneurogenesis. Neuroscience. 2012:223285–223295.

Mizutani A, et al. Boat, an AXH domain protein, suppresses the cytotoxicity of mutant ataxin-1. EMBO J. 2005; 2418:3339–3351. [PubMed: 16121196]

Orr HT, et al. Expansion of an unstable trinucleotide CAG repeat in spinocerebellar ataxia type 1. Nat. Genet. 1993; 43:221–226. [PubMed: 8358429]

Tang F, et al. MicroRNA expression profiling of single whole embryonic stem cells. Nucleic Acids Res. 2006; 342:e9. [PubMed: 16434699]

Urabe M, et al. Insect cells as a factory to produce adeno-associated virus type 2 vectors. Hum. Gene Ther. 2002; 1316:1935–1943. [PubMed: 12427305]

Velazquez-Perez L, et al. Oral zinc sulphate supplementation for six months in SCA2 patients: a randomized, double-blind, placebo-controlled trial. Neurochem. Res. 2011; 3610:1793–1800. [PubMed: 21562746]

Vig PJ, et al. Reduced immunoreactivity to calcium-binding proteins in Purkinje cells precedes onset of ataxia in spinocerebellar ataxia-1 transgenic mice. Neurology. 1998; 501:106–113. [PubMed: 9443466]

Vig PJ, et al. Relationship between ataxin-1 nuclear inclusions and Purkinje cell specific proteins in SCA-1 transgenic mice. J. Neurol. Sci. 2000; 1742:100–110. [PubMed: 10727695]

Xia H, et al. siRNA-mediated gene silencing *in vitro* and *in vivo*. Nat. Biotechnol. 2002:1006–1010. [PubMed: 12244328]

Xia H, et al. RNAi suppresses polyglutamine-induced neurodegeneration in a model of spinocerebellar ataxia. Nat. Med. 2004; 108:816–820. [PubMed: 15235598]

Zoghbi HY, Orr HT. Spinocerebellar ataxia type 1. Semin. Cell Biol. 1995; 61:29–35. [PubMed: 7620119]

Zoghbi HY, et al. Spinocerebellar ataxia: variable age of onset and linkage to human leukocyte antigen in a large kindred. Ann. Neurol. 1988; 236:580–584. [PubMed: 3165612]

Zu T, et al. Recovery from polyglutamine-induced neurodegeneration in conditional SCA1 transgenic mice. J. Neurosci. 2004; 2440:8853–8861. [PubMed: 15470152]

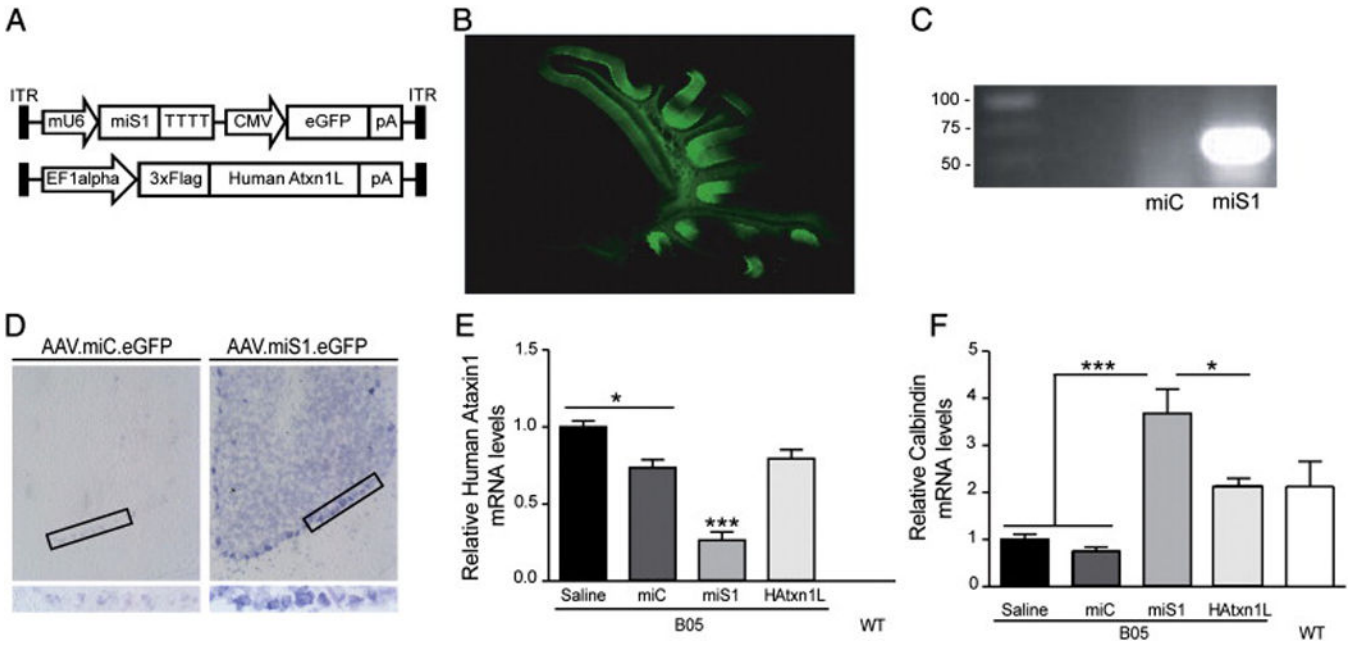

Fig. 1.

Validation of miRNA expression and silencing of human ataxin-1. A) Top depicts a cartoon of AAV2/1 vector expressing miS1 driven by the mouse U6 promoter and eGFP driven by CMV; bottom cartoon shows AAV2/1 with EF1α driving human 3× Flag-tagged ataxin-1-like. B) Sagittal section of AAV.miS1.eGFP injected mouse cerebellum. eGFP fluorescence defines AAV2/1 transduced lobules (n > 15). C) miS1 expression verified by sqPCR ($n = 4$). D) Sagittal sections of injected B05 cerebella assayed by *in situ* hybridization showing miS1 expression localized predominantly to Purkinje cells (boxed) in cerebellar cortex ($n = 3$; 3 sections/mouse). E) Quantitative PCR analysis of ataxin-1 expression in whole cerebellum showing 70% knockdown in AAV.miS1.eGFP treated mice relative to saline treated control B05 mice. F) Quantitative PCR analysis of endogenous calbindin expression in whole cerebellum showing increased levels in AAV.miS1.eGFP treated mice compared to all other treated B05 mice. Results are shown as mean ± SEM, normalized to saline injected B05 mice. (For panels E and F, $n = 4$ biological replicates, each assayed in triplicate, * indicates $p < 0.05$, *** indicates $p < 0.0001$).

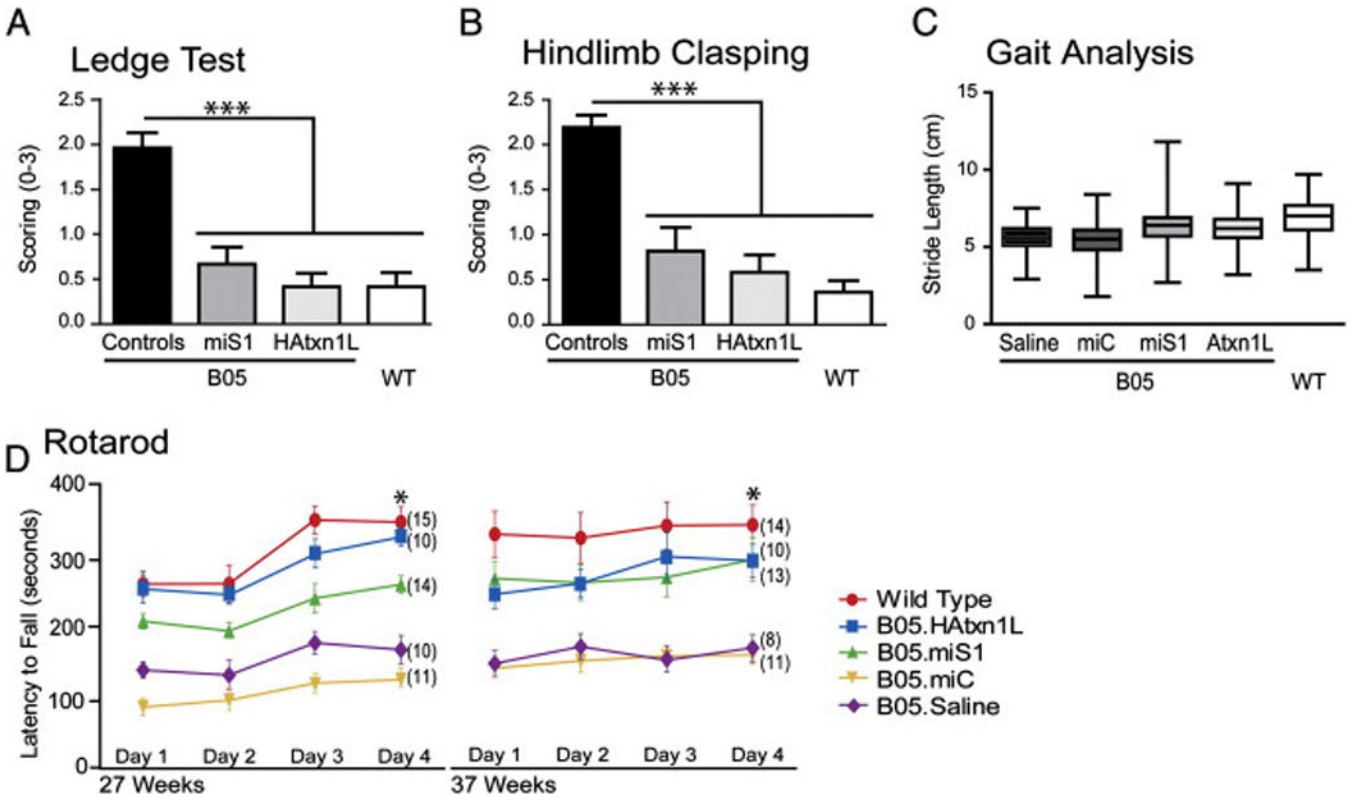

Fig. 2.

Behavioral rescue in AAV.miS1.eGFP or AAV.HAtxn1L treated mice. A) Ledge test showing AAV.miS1.eGFP injected, AAV.HAtxn1L injected and wild type mice perform significantly better than control treated B05 littermates. B) Hindlimb clasping assay showing AAV.miS1.eGFP-injected, AAV.HAtxn1L-injected and wild type mice perform significantly better than control treated B05 littermates. For panels A and B, results are shown as mean ± SEM (*** indicates $p < 0.0001$). Uninjected wild type, $n = 14$; control (AAV.miC and saline) injected B05, $n = 26$; AAV.miS1 injected B05, $n = 11$; AAV.HAtxn1L injected B05, $n = 12$ mice. C) Box plots showing AAV.miS1.eGFP and AAV.HAtxn1L treated mice have significantly longer stride lengths than control injected B05 littermates. Measurements from 16 to 20 steps per mouse (11–14 mice per treatment group) were averaged for all four paws. D) Rotarod performance at 27 and 37 weeks of age. At both time points, AAV.miC.eGFP and saline injected B05 littermates perform significantly worse than therapeutically treated and wild type mice (* indicates $p < 0.05$, the number of mice per group is indicated in parentheses).

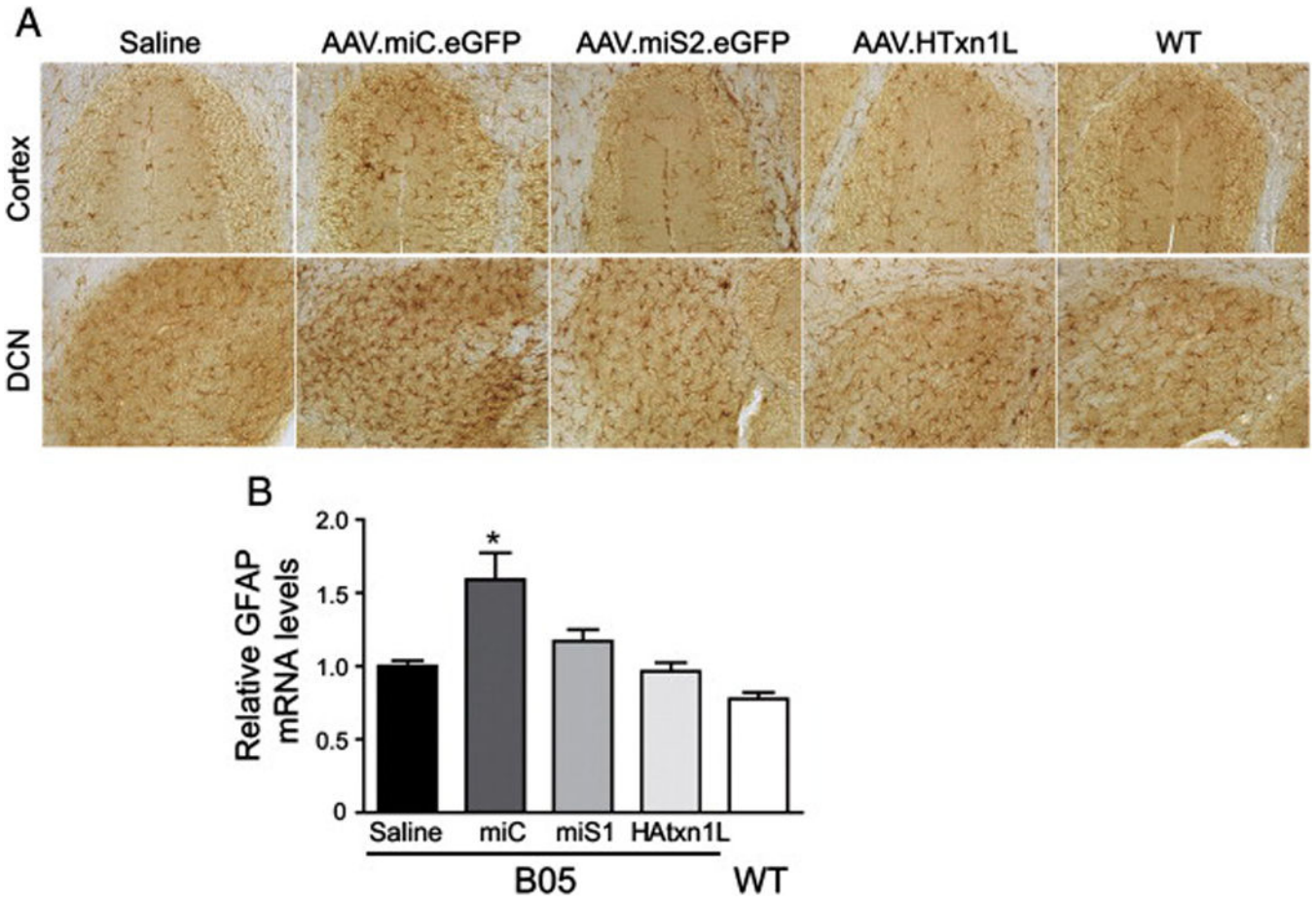

Fig. 3.

AAV.miS1.eGFP and AAV.HAtxn1L treated animals show no adverse microglia or astroglia activation in the cerebellum. A) Sagittal 60 μm-thick representative cerebellar sections from all groups were stained for the microglia activation marker Iba1. Top panels show Iba1 levels in comparable sections of cerebellar cortex. Bottom panels show Iba1 levels at the injection site in the DCN. No gross difference in the amount of microglia activation was seen between wild type animals and individual treatment groups (n = 3 mice per treatment group; 1–3 sections per mouse were evaluated). B) Quantitative PCR was used to quantify relative GFAP expression levels, an astroglia marker. No significant differences were seen between therapeutic treatment groups and saline treated animals. However, AAV.miC.eGFP injected B05 animals had higher levels of GFAP than all other groups. Results are shown as mean ± SEM (n = 4 mice per treatment group; samples assayed in triplicate, * indicates $p < 0.05$).

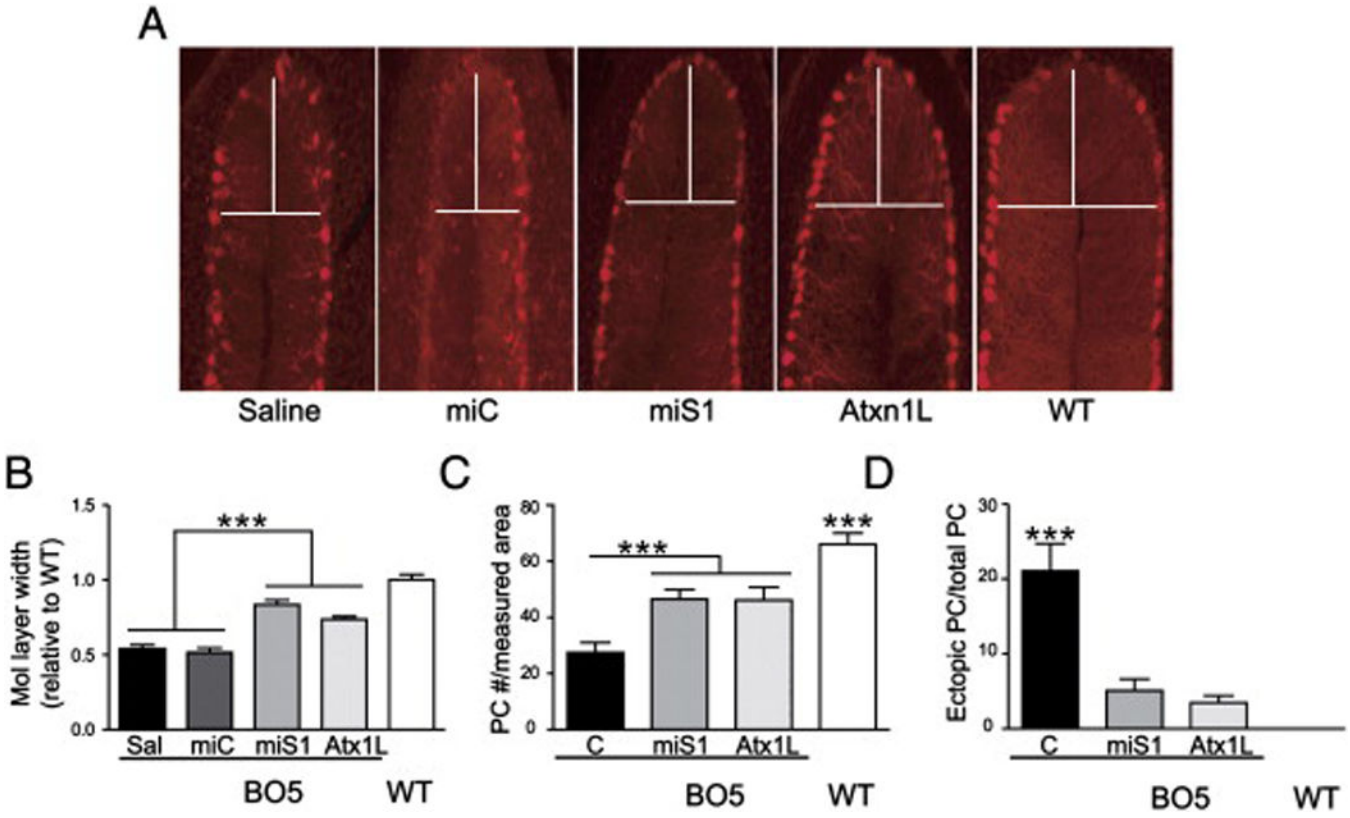

Fig. 4.

Molecular rescue of Purkinje cells in the cerebellum. A) Sagittal 60 μm-thick representative cerebellar sections from all groups were stained for the Purkinje cell marker, calbindin. B) Molecular layer widths relative to WT mice. Mice treated with AAV.miS1.eGFP and AAV.HAtxn1L had significantly wider molecular layers than control treated B05 littermates. The molecular layer widths between lobules IV–V and VI were quantified in the region indicated by horizontal white lines. C) Purkinje cell counts per unit area. AAV.miS1.eGFP and AAV.HAtxn1L treated mice had significantly more Purkinje cells than control treated B05 littermates. D) Ratio of ectopic Purkinje cells to total number of Purkinje cells per unit area. Control treated B05 mice had a significantly higher ratio of ectopic Purkinje cells to total Purkinje cells compared to all other treatment groups. Results are shown as mean ± SEM (for panels B–D, $n = 3$ mice per treatment group; 1–3 sections per mouse were quantified), ** indicated $p < 0.001$; *** indicated $p < 0.0001$).